PROTEIN STRUCTURE REPORT

Solution structures and backbone dynamics of the ribosomal protein S6 and its permutant P^{54-55}

Anders Öhman,[1]* Tommy Öman,[1] and Mikael Oliveberg[2]

[1]Department of Chemistry, Umeå University, Umeå SE-901 87, Sweden

[2]Department of Biochemistry and Biophysics, Arrhenius Laboratories of Natural Sciences, Stockholm University, Stockholm SE-106 91, Sweden

Received 20 October 2009; Accepted 4 November 2009
DOI: 10.1002/pro.298
Published online 20 November 2009 proteinscience.org

Abstract: The ribosomal protein S6 from *Thermus thermophilus* has served as a model system for the study of protein folding, especially for understanding the effects of circular permutations of secondary structure elements. This study presents the structure of a permutant protein, the 96-residue P^{54-55}, and the structure of its 101-residue parent protein $S6^{wt}$ in solution. The data also characterizes the effects of circular permutation on the backbone dynamics of S6. Consistent with crystallographic data on $S6^{wt}$, the overall solution structures of both P^{54-55} and $S6^{wt}$ show a β-sheet of four antiparallel β-strands with two α-helices packed on one side of the sheet. In clear contrast to the crystal data, however, the solution structure of $S6^{wt}$ reveals a disordered loop in the region between β-strands 2 and 3 (Leu43-Phe60) instead of a well-ordered stretch and associated hydrophobic mini-core observed in the crystal structure. Moreover, the data for P^{54-55} show that the joined wild-type N- and C-terminals form a dynamically robust stretch with a hairpin structure that complies with the *in silico* design. Taken together, the results explain why the loop region of the $S6^{wt}$ structure is relatively insensitive to mutational perturbations, and why P^{54-55} is more stable than $S6^{wt}$: the permutant incision at Lys54-Asp55 is energetically neutral by being located in an already disordered loop whereas the new hairpin between the wild-type N- and C-termini is stabilizing.

Keywords: NMR solution structure; backbone dynamics; S6; permutant; folding

Introduction

The ribosomal protein S6 is one component of the small subunit of the ribosome,[1] known to be important for the assembly of the central domain of the small subunit via heterodimerization with S18.[2] The crystal structure of the 101 amino acid protein S6 from *Thermus thermophilus* shows that it folds into a core composed of two β-α-β secondary structure motifs, forming a four-stranded antiparallel β-sheet with the two α-helices assembled on one side of the sheet.[3] From this core, a hook-region of conserved residues extends as two antiparallel β-

Additional Supporting Information may be found in the online version of this article.

Abbreviations: NMR, nuclear magnetic resonance; NOE, nuclear Overhauser effect; RMSD, root mean square deviation.

Grant sponsor: Sven och Lily Lawskis Stiftelse, Magn. Bergvalls Foundation, Carl Trygger Foundation, Bernhard och Signe Bäckströms Stiftelse, O.E. och Edla Johanssons Vetenskapliga Stiftelse, Göran Gustafssons Foundation, K. and A. Wallenberg foundation and Swedish Research Science Council.

*Correspondence to: Anders Öhman, Department of Chemistry, Umeå University, Umeå SE-901 87, Sweden.
E-mail: anders.ohman@chem.umu.se

Table I. *Structural Statistics for the Ensembles of 20 Structures of $S6^{wt}$ and P^{54-55}*

	$S6^{wt}$	P^{54-55}
Number of NOE-derived distance restraints		
Total number	745	770
Intraresidue	252	213
Sequential ($\|i-j\|=1$)	307	303
Medium range ($2 \leq \|i-j\| \leq 4$)	97	138
Long range ($\|i-j\| \geq 5$)	89	116
Number of dihedral angle restraints		
Backbone ϕ-angle	90	88
Backbone ψ-angle	65	65
Average number of violations		
Distance restraints >0.5 Å	0	0
Dihedral angle restraints >5°	0	0
Deviations from idealized covalent geometry		
Bonds (Å)	0.0022 ± 0.0001	0.0032 ± 0.0001
Angles (°)	0.54 ± 0.01	0.57 ± 0.01
Impropers (°)	0.39 ± 0.01	0.44 ± 0.01
Ramachandran plot analysis, residues	3–42, 59–91	6–85
Most favored regions (%)	95.0	84.1
Additionally allowed regions (%)	4.9	14.5
Generously allowed regions (%)	0.1	1.3
Disallowed regions (%)	0.0	0.0
Atomic RMSD, residues	3–42, 59–91	6–85
Backbone heavy atoms (Å)	0.95	0.66
All heavy atoms (Å)	1.60	1.44
PDB-ID	2KJV	2KJW

strands, forming a mini-core of hydrophobic residues.[2,4–6]

S6 has been extensively characterized with respect to its folding properties[7,8] and, in particular, how folding is affected by circular permutations, that is how changes in the order of secondary structure elements affect the folding process.[9] Detailed ϕ-value analysis on a number of engineered permutants of S6 reveals that there are two competing folding nuclei, both with analogous structural outline but where the first nucleus (σ1) consists of β1-α1-β3 and the second nucleus (σ2) of β1-α2-β4. As a consequence of the two folding nuclei, the folding of S6 can occur on two parallel pathways with opposite folding order. $S6^{wt}$ is mainly biased towards the σ1 pathway, whereas the permutant P^{54-55} favors the σ2 pathway.[9–11]

In this study, we use NMR spectroscopy to characterize the structure and dynamics of $S6^{wt}$ and P^{54-55} in solution. The results presented here shed new light on how circular permutations affect protein structure, dynamics, and stability.

Results and Discussion

The assigned ^{15}N-HSQC spectra for S6 and P^{54-55} show well dispersed peaks as expected for folded proteins (Supporting Information Fig. S1). For both proteins, nearly complete backbone assignments and extensive side-chain assignments were obtained. $S6^{wt}$ has a second set of peaks for Ala53 and Leu98. Since these residues are located in the vicinity of Pro51, Pro56, and Pro96, the second set of peaks may be due to proline cis-trans isomerization; the smaller fraction was estimated to ~20% or less as judged from the relative peak intensities. In addition, the C-terminal residues Asn100 and Ala101 cannot be resolved due to overlapping chemical shifts. P^{54-55} displays a set of duplicate peaks of approximately equal intensity for Asp2, presumably due to cis-trans interconversion of the subsequent residue, Pro3. The C-terminal residues of P^{54-55} are also likely to be significantly affected by the presence of a proline at position 93 (Pro93). Ala95 and Lys96 have triplicate or quadruple peaks, where the major conformer has occupancy of 50–60%. Resonances for Tyr92 and Ile94 were not observed in the ^{15}N-HSQC spectrum, probably due to exchange broadening. In addition, the chemical shifts of Leu90 and Ala91 vary with sample preparation.

A total of 745 and 770 nonredundant distance restraints were determined for $S6^{wt}$ and P^{54-55}, respectively (Table I). Dihedral angle restraints were derived, in part, from HNHA experiments using the analysis program Mulder. In addition, the program TALOS provided 65 pairs of backbone (ϕ,ψ) dihedral angle restraints for both proteins, which was classified as Good by TALOS (Table I). The TALOS-derived restraints were selected only if they were in agreement with the ϕ-values provided by Mulder. An additional eight ($S6^{wt}$) and seven (P^{54-55}) ϕ-angles for nonglycine residues were restrained to

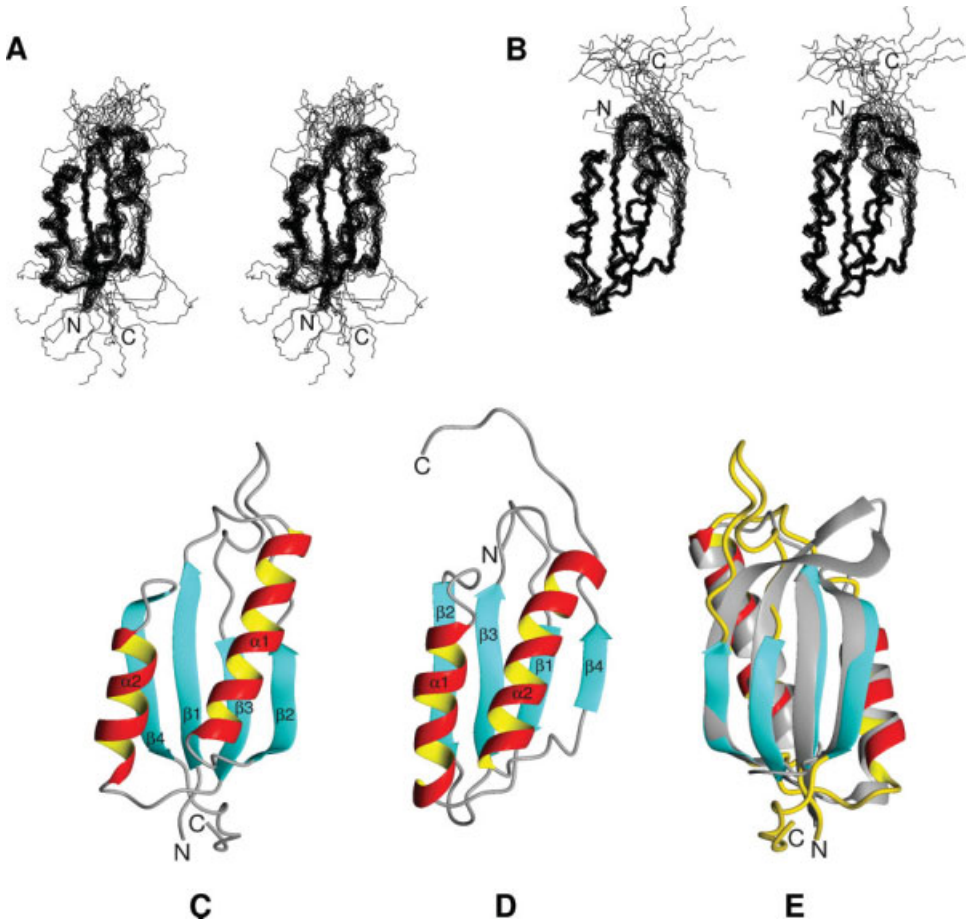

Figure 1. Solution structures of $S6^{wt}$ and P^{54-55}. Stereo views of (A) $S6^{wt}$ and (B) P^{54-55} solution structures, showing the backbone trace for the final ensembles of 20 calculated structures (PDB-IDs: 2KJV and 2KJW, respectively). The secondary structure regions are superimposed and their N- and C-termini are indicated. Ribbon representations of the lowest-energy structures of (C) $S6^{wt}$ and (D) P^{54-55}, in which the N- and C-terminals as well as secondary structure elements are identified. (E) The solution structure of $S6^{wt}$ (depicted in color) superimposed onto the crystal structure (in grey; PDB-ID: 1RIS). The structures in panel (E) are rotated 180° around a vertical axis compared to the structure in panel (C).

negative values,[12] based on weak intraresidue NOEs between HN and Hα protons. From the structure calculations, 54 of 300 structures and 53 of 200 structures were accepted for $S6^{wt}$ and P^{54-55}, respectively. The final ensembles consisted of 20 structures [Fig. 1(A and B)] that were selected based on their energies and Ramachandran behavior. Structural statistics are presented in Table I, and ribbon structures of representative conformers of $S6^{wt}$ and P^{54-55} are presented in Figure 1(C and D).

The solution structure of $S6^{wt}$ has a well-defined core, containing a β-sheet of four antiparallel β-strands and two α-helices packed on one side of the sheet, as well as a flexible loop and C-terminal, see Figure 1(A and C). The connectivity scheme of the secondary structure elements is β1-α1-β2-β3-α2-β4. The N-terminal residues (Met1-Arg3) are followed by the first β-strand (β1, Tyr4-Leu10), a turn (Asn11-Asp15), the first α-helix (α1, Gln16-Asn32), a turn (Tyr33-Arg36), the second β-strand (β2, Val37-Glu42), an 18-residue loop (Leu43-Phe60), the third β-strand (β3, Leu61-Val65) packed antiparallel in between strand β1 and β2, a turn (Glu66-Asp70), the second α-helix (α2, Arg71-Ile81), a turn (Arg82-Asn84), the fourth β-strand (β4, Val85-Val91) packed antiparallel to β1, followed by nine disordered C-terminal residues (Lys92-Ala101). The atomic RMSD:s for the backbone and heavy atoms of residues 3–42 and 59–91 in the ensemble of $S6^{wt}$ structures are 0.95 and 1.6 Å, respectively (Table I).

Similar to its parent structure, the solution structure of the designed permutant protein P^{54-55} has a well-defined core structure containing a β-sheet of four antiparallel β-strands and two α-helices packed on one side of the sheet [Fig. 1(B and D)]. As intended by the design of the permutant, the secondary structure connectivity is β1-α1-β2-β3-α2-β4 (or with the nomenclature of $S6^{wt}$: β3-α2-β4-β1-α1-β2). The N-terminal residues (Met1-Phe7), which are disordered, are followed by the first β-strand (β2, Leu8-Tyr10), a turn (Gln11-Pro15), the first α-helix (α1, Glu16-Ile28), a turn (Arg29-Arg33), the second β-strand (β2, Arg34-

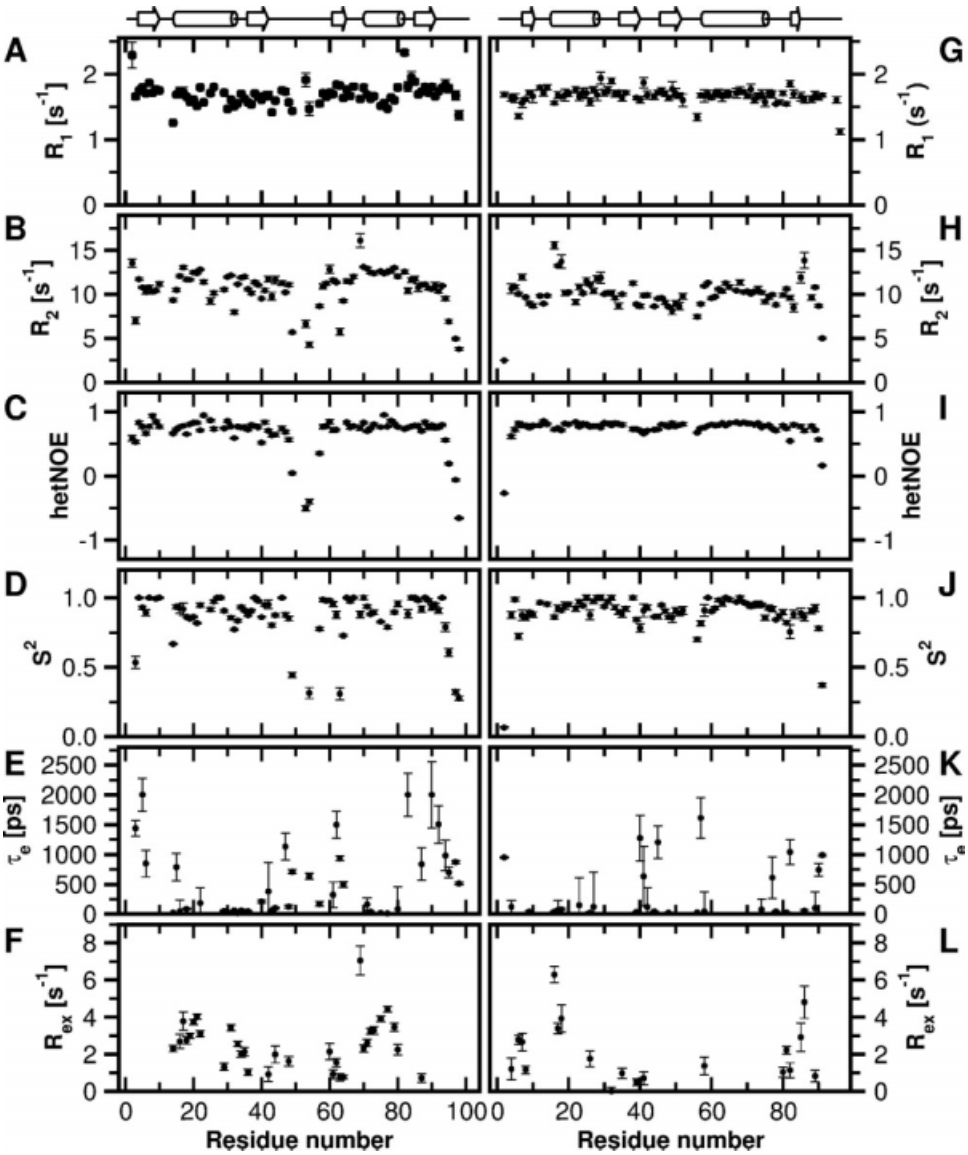

Figure 2. Backbone dynamics of $S6^{wt}$ and P^{54-55}. Backbone ^{15}N NMR relaxation data and motional parameters for (A–F) $S6^{wt}$ and (G–L) P^{54-55} at 25°C and at 14.1 T, plotted as a function of residue number. Longitudinal relaxation rate constants are shown in (A and G), transverse relaxation rate constants in (B and H), and $\{^1H\}$-^{15}N NOEs in (C and I). Order parameters (S^2), effective internal correlation times (τ_e) and exchange rates (R_{ex}) are shown in (D and J), (E and K), and (F and L), respectively.

Ala39), a turn (Ser40-Arg45), the third β-strand (β3, Tyr46-Val51) packed antiparallel in between strand β1 and β2, a turn (Leu52-Asp57), the second α-helix (α2, Gln58-Tyr75), a turn (Gly76-Lys81), the fourth β-strand (β4, Val82-Glu84) packed antiparallel with β1, followed by less well-defined C-terminal residues (Leu85-Lys96). The atomic RMSD:s for the backbone and heavy atoms of residues 6–85 in the ensemble of P^{54-55} structures are 0.66 and 1.44 Å, respectively (Table I). The core of the P^{54-55} solution structure is fairly similar to the solution structure of $S6^{wt}$; their lowest-energy structures have a RMSD of 2.57 Å for the backbone atoms of residues Tyr6-Val38 and Arg45-Glu84 in P^{54-55} compared with the corresponding residues Tyr59-Val91 and Arg3-Glu42 in $S6^{wt}$ [Fig. 1(C and D)].

The backbone dynamics of $S6^{wt}$ were characterized by measurements of ^{15}N R_1, R_2 and $\{^1H\}$-^{15}N NOE [Fig. 2 (A–C)]. In particular the R_2 and $\{^1H\}$-^{15}N NOE data demonstrate the dynamic properties of the loop (Leu43-Phe60) and the C-terminal (Ser93-Ala101). From the model-free analysis of the relaxation data, a rotational correlation time of 7.3 ns and a diffusion tensor ratio of 0.76 were derived. Many residues (25 of 75) were fitted by model i, 15 by model ii, 9 by model iii, 23 by model iv, and 3 by model v. Overall, residues in secondary structure elements display high ^1H-^{15}N order parameter (S^2), with an average of 0.91 [Fig. 2(D)]. In addition, a number of residues exhibit substantial dynamics on the picosecond-nanosecond timescale [Fig. 2(E)] and chemical exchange on the millisecond timescale [Fig. 2(F)].

Measurement of backbone dynamics for P^{54-55} demonstrates that the N- and C-terminal residues are disordered [Fig. 2(G–I)]. Model-free analysis of the relaxation data yielded a rotational correlation time of 6.9 ns and a diffusion tensor ratio of 0.80. Relaxation data for a majority of the residues (42 of 79) were described by model i, 9 by model ii, 7 by model iii, 12 by model iv, and 9 by model v. The H—N order parameters for P^{54-55} are high overall, with an average of 0.92 for residues in secondary structure elements [Fig. 2(J)]. In comparison to $S6^{wt}$, the permutant has less number of residues that display dynamics on the picosecond timescale [Fig. 2(K)] and chemical exchange on the millisecond timescale [Fig. 2(L)].

The core of the solution structure of $S6^{wt}$ is very similar to that of the crystal structure (PDB-ID: 1RIS),[3] with a RMSD of 1.60 Å for the backbone atoms of residues Arg3-Glu42 and Tyr59-Val91, using the lowest-energy solution structure for comparison [Fig. 1(E)]. The main differences are observed in the end of β-strand β2 and in the beginning of strand β3, which are flexible in solution [Fig. 1(A)]. The flexible properties of the loop-region (Leu43-Phe60) are clearly revealed by the relaxation measurements [Fig. 2(A–F)], where these residues exhibit lower than average R_2 values and order parameters, and negative heteronuclear NOEs. The lack of high crystallographic B-factors in this region further confirms this difference (Supporting Information Fig. S2). The crystal structures of $S6^{wt}$ alone or within the ribosome are very similar and show that this loop-region (or so-called hook-region[3]) forms two well-defined antiparallel β-strands, creating a mini-core of hydrophobic residues. The mini-core appears to be important for protein–protein interactions, either for the crystal packing of $S6^{wt}$ itself or for the interaction with S18 within the ribosome. In a previous folding study,[8] two point-mutations, I48A and L52A, were introduced within the assumed mini-core [Fig. 3 (A)], without an expected destabilization of the protein [see the chevron plots in Fig. 3(B)]. The solution structure shows that these sites of mutation are located in a loop-region that is flexible instead of an ordered mini-core. As a result, these mutations have negligible effects on protein stability. In contrast, the chevron plot in Figure 3(B) further reveals a clear difference in stability between $S6^{wt}$ and P^{54-55}. The overall more rigid core structure for P^{54-55} and the additional hairpin structure between the original N- and C-termini may account for the 0.49 kcal/mol higher stability of the permutant compared to $S6^{wt}$.

In conclusion, the structure and dynamic properties of $S6^{wt}$ in solution explain the insensitivity of mutations in the hook region to overall stability. These results show that this region is more flexible or dynamic in solution than the hydrophobic mini-core defined by the crystal structure. Secondly, the solution structure of P^{54-55}, which to our knowledge represents the first three-dimensional solution structure of a permutant protein, shows that the permutation process itself does not affect the overall three-dimensional structure. Moreover, the conformational dynamics of the permutant protein are reduced overall, which provides new insight into its increased global stability. These results set the basis for further analysis of the dynamic properties of $S6^{wt}$ and engineered permutants of S6 by NMR to accompany the wealth of protein folding and stability data already available for this model system.[7,8]

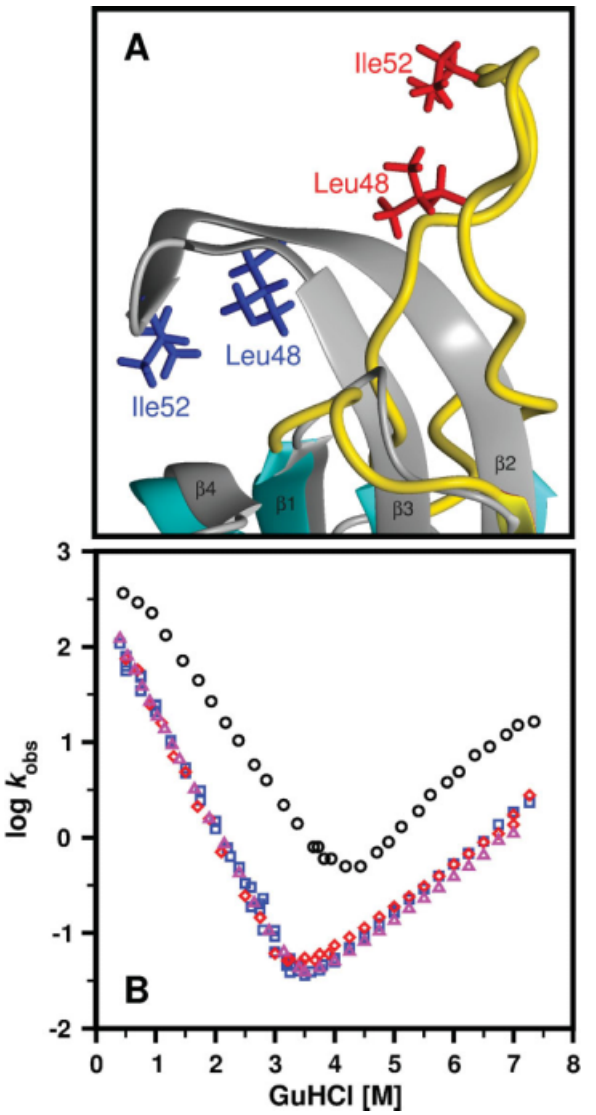

Figure 3. Loop-region of $S6^{wt}$ and chevron plots of $S6^{wt}$, S6 mutants and P^{54-55}. (A) The loop-region of the $S6^{wt}$ solution structure (depicted in color) superimposed onto the crystal structure (in grey; PDB-ID: 1RIS), where the mutated residues, Leu48 and Ile52, are indicated. (B) Chevron plots of $S6^{wt}$ (blue squares), the mutant L48A (red diamonds), the mutant I52A (magenta triangles) and P^{54-55} (black rings). The data are adapted from[8,11] whereas the chevron plots of the L48A and I52A mutants are not previously published.

Materials and Methods

Sample preparation

Cloning, expression and purification of $S6^{wt}$ and P^{54-55} were carried out as previously described.[7,9–11] Lyophilized proteins were dissolved in a solvent containing 20 m*M* MES, pH 6.3, 50 m*M* NaCl and 10% (v/v) D_2O, to a concentration of ~0.5 m*M*.

NMR spectroscopy

NMR experiments for chemical shift assignments, structure calculations, and backbone dynamics were collected at 25°C on a 600 MHz Bruker AVANCE spectrometer, equipped with a 5 mm triple-resonance, pulsed-field z-gradient warm or cryogenically cooled probe. Recorded datasets were processed using NMRPipe[13] or XWINNMR/Topspin (Bruker Biospin) and resonance assignments were determined with Ansig for Windows.[14] The sequence specific resonance assignments followed the standard assignment strategy[15] and were based on 2D ^{15}N-HSQC, 3D ^{15}N-edited NOESY-HSQC, and DIPSI-HSQC, as well as a standard set of 3D triple resonance experiments.[16] Backbone and partial side-chain assignments of P^{54-55} were obtained from CBCANH, CBCA(CO)NH, HNCO, HSQC, HNCA, and HN(CO)CA experiments, while the side-chain assignments were verified and extended using 2D clean-TOCSY and DQF-COSY and 3D ^{15}N-edited DIPSI-HSQC, C(CO)NH, HC(CO)NH, and HCCH-TOCSY experiments. Distance restraints were obtained from 3D ^{15}N-edited NOESY experiments with a mixing time of 100 ms. Dihedral angle restraints were derived from scalar coupling constants measured in HNHA experiments.

Structural restraints

The analysis of the NOESY spectra resulted in a set of unambiguously assigned NOEs, which were calibrated to known distances found in both α-helical and β-sheet secondary structure elements. The NOE-based restraints were divided into three classes: strong (1.8–2.7 Å), medium (1.8–3.6 Å) and weak (1.8–5.5/6.0 Å). By using an iterative combination of structure calculation and a set of unambiguous distance restraints, many ambiguous NOE cross-peaks were resolved and assigned. The obtained distance restraints were processed by AQUA to remove redundant restraints.[17] Dihedral angle restraints were derived from coupling constants using the Mulder program[18] and chemical shifts using the TALOS program.[19]

Structure calculation and analysis

Structures were calculated and analyzed using XPLOR, (v. 3.851). Additional structural analysis and molecular visualization were carried out using MOLMOL[20] and Procheck-NMR.[17] A total number of 200 (P^{54-55}) or 300 ($S6^{wt}$) structures were calculated from the structural restraints, using the XPLOR scripts sa.inp and two rounds of refine.inp. The duration of the first high-temperature molecular dynamics step in the sa.inp protocol was increased to 45 ps, while the annealing step was increased to 30 ps. Similarily, the duration of the simulated annealing in the refinement protocol was increased to 30 ps. Distance restraints for nonstereo specifically assigned protons were included using r^{-6} summation.[21] Selection of calculated structures was based on the criteria in the XPLOR script accept.inp (RMSD for bonds and angles less than 0.01 Å and 1°, respectively; no NOE violation larger than 0.5 Å and no dihedral angle restraint violation larger than 5°).

Backbone dynamics

Experiments for measurement of ^{15}N longitudinal and transverse relaxation rate constants and {^{1}H}-^{15}N steady state NOE were recorded as described previously.[22] For backbone amide ^{15}N longitudinal relaxation rate constants, R_1, two-dimensional correlation spectra were measured for 11 different relaxation delays: 0, 0.010, 0.050, 0.120, 0.220, 0.350, 0.510, 0.700, 0.920, 1.170, and 1.450 s. Transverse relaxation rate constants, R_2, were determined correlation spectra measured with 10 different relaxation delays: 0, 0.017, 0.034, 0.050, 0.067, 0.084, 0.101, 0.134, 0.168, 0.202 s. {^{1}H}-^{15}N steady state NOE experiments were recorded in an interleaved manner with and without ^{1}H saturation during the 5 second recycle delay. Relaxation rate constants were determined from the single exponential decay of peak intensities in correlation spectra using NMRView[23] and Grace (http://plasma-gate.weizmann.ac.il/Grace), while steady-state NOE values were determined in NMRView from the ratio of peak-heights for spectra recorded with and without ^{1}H saturation.

The inertia and diffusion tensors of representative structures of $S6^{wt}$ and P^{54-55} were determined using the programs pdbinertia and r2r1_diffusion,[24] respectively (A.G. Palmer, Columbia University; http://www.palmer.hs.columbia.edu/software/diffusion.html). ^{15}N relaxation data were analyzed with the Lipari-Szabo model-free formalism, using Modelfree (v4.2)[25,26] and the Fast-Modelfree interface[27]. Each N—H pair was evaluated using the following models for internal motion: (i) S^2, (ii) S^2 and τ_e, (iii) S^2 and R_{ex}, (iv) S^2, τ_e, and R_{ex}, and, (v) S_f^2, S^2, and τ_e, where S^2 and S_f^2 denote the generalized order parameter and the order parameter for fast internal motion, respectively, τ_e is the effective internal correlation time, and R_{ex} the exchange of transverse relaxation.

Accession numbers

The sequence specific resonance assignments of $S6^{wt}$ and P^{54-55} have been deposited in the BioMagResBank (accession numbers: BMRB-16344 and BMRB-16345). Coordinates of the final ensembles of 20 structures of

$S6^{wt}$ and P^{54-55} have been deposited in the Protein Data Bank (PDB ID-codes: 2KJV and 2KJW).

References

1. Steitz TA (2008) A structural understanding of the dynamic ribosome machine. Nat Rev Mol Cell Biol 9:242–253.
2. Agalarov SC, Sridhar Prasad G, Funke PM, Stout CD, Williamson JR (2000) Structure of the S15,S6,S18-rRNA complex: assembly of the 30S ribosome central domain. Science 288:107–113.
3. Lindahl M, Svensson LA, Liljas A, Sedelnikova SE, Eliseikina IA, Fomenkova NP, Nevskaya N, Nikonov SV, Garber MB, Muranova TA, Rykanova AI, Amons R (1994) Crystal structure of the ribosomal protein S6 from *Thermus thermophilus*. Embo J 13:1249–1254.
4. Schluenzen F, Tocilj A, Zarivach R, Harms J, Gluehmann M, Janell D, Bashan A, Bartels H, Agmon I, Franceschi F, Yonath A (2000) Structure of functionally activated small ribosomal subunit at 3.3 angstroms resolution. Cell 102:615–623.
5. Wimberly BT, Brodersen DE, Clemons WM, Jr, Morgan-Warren RJ, Carter AP, Vonrhein C, Hartsch T, Ramakrishnan V (2000) Structure of the 30S ribosomal subunit. Nature 407:327–339.
6. Yusupov MM, Yusupova GZ, Baucom A, Lieberman K, Earnest TN, Cate JH, Noller HF (2001) Crystal structure of the ribosome at 5.5 A resolution. Science 292: 883–896.
7. Otzen DE, Kristensen O, Proctor M, Oliveberg M (1999) Structural changes in the transition state of protein folding: alternative interpretations of curved chevron plots. Biochemistry 38:6499–6511.
8. Otzen DE, Oliveberg M (2002) Conformational plasticity in folding of the split beta-alpha-beta protein S6: evidence for burst-phase disruption of the native state. J Mol Biol 317:613–627.
9. Lindberg M, Tangrot J, Oliveberg M (2002) Complete change of the protein folding transition state upon circular permutation. Nat Struct Biol 9:818–822.
10. Haglund E, Lindberg MO, Oliveberg M (2008) Changes of protein folding pathways by circular permutation. Overlapping nuclei promote global cooperativity. J Biol Chem 283:27904–27915.
11. Lindberg MO, Haglund E, Hubner IA, Shakhnovich EI, Oliveberg M (2006) Identification of the minimal protein-folding nucleus through loop-entropy perturbations. Proc Natl Acad Sci USA 103:4083–4088.
12. Ludvigsen S, Poulsen FM (1992) Positive theta-angles in proteins by nuclear magnetic resonance spectroscopy. J Biomol NMR 2:227–233.
13. Delaglio F, Grzesiek S, Vuister GW, Zhu G, Pfeifer J, Bax A (1995) NMRPipe: a multidimensional spectral processing system based on UNIX pipes. J Biomol NMR 6:277–293.
14. Helgstrand M, Kraulis P, Allard P, Härd T (2000) Ansig for Windows: an interactive computer program for semiautomatic assignment of protein NMR spectra. J Biomol NMR 18:329–336.
15. Wüthrich K (1986) NMR of proteins and nucleic acids. New York: John Wiley & Sons.
16. Sattler M, Schleucher J, Griesinger C (1999) Heteronuclear multidimensional NMR experiments for the structure determination of proteins in solution employing pulsed field gradients. Prog NMR Spectrosc 34:66.
17. Laskowski RA, Rullmannn JA, MacArthur MW, Kaptein R, Thornton JM (1996) AQUA and PROCHECK-NMR: programs for checking the quality of protein structures solved by NMR. J Biomol NMR 8:477–486.
18. Padrta P, Sklenar V (2002) Program MULDER—a tool for extracting torsion angles from NMR data. J Biomol NMR 24:339–349.
19. Cornilescu G, Delaglio F, Bax A (1999) Protein backbone angle restraints from searching a database for chemical shift and sequence homology. J Biomol NMR 13:289–302.
20. Koradi R, Billeter M, Wüthrich K (1996) MOLMOL: a program for display and analysis of macromolecular structures. J Mol Graph 14:51–55, 29–32.
21. Fletcher CM, Jones DNM, Diamond R, Neuhaus D (1996) Treatment of NOE constraints involving equivalent or nonstereoassigned protons in calculations of biomacromolecular structures. J Biomol NMR 8:19.
22. Farrow NA, Muhandiram R, Singer AU, Pascal SM, Kay CM, Gish G, Shoelson SE, Pawson T, Forman-Kay JD, Kay LE (1994) Backbone dynamics of a free and phosphopeptide-complexed Src homology 2 domain studied by 15N NMR relaxation. Biochemistry 33: 5984–6003.
23. Johnson BA, Blevins RA (1994) NMRView: a computer program for the visualization and analysis of NMR data. J Biomolecular NMR 4:603–614.
24. Lee LK, Rance M, Chazin WJ, Palmer AG, III (1997) Rotational diffusion anisotropy of proteins from simultaneous analysis of 15N and 13C alpha nuclear spin relaxation. J Biomol NMR 9:287–298.
25. Mandel AM, Akke M, Palmer AG, III (1995) Backbone dynamics of *Escherichia coli* ribonuclease HI: correlations with structure and function in an active enzyme. J Mol Biol 246:144–163.
26. Palmer AG, Rance M, Wright PE (1991) Intramolecular motions of a zinc finger DNA-binding domain from Xfin characterized by proton-detected natural abundance carbon-13 heteronuclear NMR spectroscopy. JACS 113:10.
27. Cole R, Loria JP (2003) FAST-Modelfree: a program for rapid automated analysis of solution NMR spin-relaxation data. J Biomol NMR 26:203–213.